



Published in final edited form as:

J Neural Eng. 2018 October ; 15(5): 056006. doi:10.1088/1741-2552/aacdb9.

Optogenetic entrainment of neural oscillations with hybrid fiber probes

Antje Kilias^{1,2,3,†}, Andres Canales^{4,†}, Ulrich P. Froriep^{4,5,6,†}, Seongjun Park⁷, Ulrich Egert^{1,2,*}, and Polina Anikeeva^{4,*}

¹Bernstein Center Freiburg, University of Freiburg, Freiburg, Germany

²Biomicrotechnology, Institute for Microsystems Engineering, University of Freiburg, Freiburg, Germany

³Faculty of Biology, University of Freiburg, Freiburg, Germany

⁴Department of Materials Science and Engineering, and Research Laboratory of Electronics, Massachusetts Institute of Technology, Cambridge, MA, USA

⁵Simons Center for the Social Brain, Massachusetts Institute of Technology, Hannover, Germany

⁶Fraunhofer Institute for Toxicology and Experimental Medicine, Hannover, Germany

⁷Department of Electrical Engineering and Computer Science, and Research Laboratory of Electronics, Massachusetts Institute of Technology, Cambridge, MA, USA

Abstract

Objective—Optogenetic modulation of neural activity is a ubiquitous tool for basic investigation of brain circuits. While the majority of optogenetic paradigms rely on short light pulses to evoke synchronized activity of optically sensitized cells, many neurobiological processes are associated with slow local field potential (LFP) oscillations. Therefore, we developed a hybrid fiber probe capable of simultaneous electrophysiological recording and optical stimulation and used it to investigate the utility of sinusoidal light stimulation for evoking oscillatory neural activity *in vivo* across a broad frequency range.

Approach—We fabricated hybrid fiber probes comprising a hollow cylindrical array of 9 electrodes and a flexible optical waveguide integrated within the core. We implanted these probes in the hippocampus of transgenic Thy1-ChR2-YFP mice that broadly express the blue-light sensitive cation channel channelrhodopsin 2 (ChR2) in excitatory neurons across the brain. The effects of the sinusoidal light stimulation were characterized and contrasted with those corresponding to pulsed stimulation in the frequency range of physiological LFP rhythms (3 – 128 Hz).

Main results—Within hybrid probes, metal electrode surfaces were vertically aligned with the waveguide tip, which minimized optical stimulation artifacts in neurophysiological recordings. Sinusoidal stimulation resulted in reliable and coherent entrainment of LFP oscillations up to 70

*All correspondence should be addressed to U.E. (egert@imtek.uni-freiburg.de) and P.A. (anikeeva@mit.edu).

†These authors have contributed equally

Hz, the cutoff frequency of ChR2, with response amplitudes inversely scaling with the stimulation frequencies. Effectiveness of the stimulation was maintained for two months following implantation.

Significance—Alternative stimulation patterns complementing existing pulsed protocols, in particular sinusoidal light stimulation, are a prerequisite for investigating the physiological mechanisms underlying brain rhythms. So far, studies applying sinusoidal stimulation *in vivo* were limited to single stimulation frequencies. We show the feasibility of sinusoidal stimulation *in vivo* to induce coherent LFP oscillations across the entire frequency spectrum supported by the gating dynamics of ChR2 and introduce a hybrid fiber probe tailored to continuous light stimulation.

Keywords

hybrid probe; optical stimulation; hippocampus; channelrhodopsin 2; sinusoidal; local field potential; network rhythms

1. Introduction

With its millisecond temporal resolution and genetic cell-type specificity, optogenetics has become a go-to tool for manipulation of neural activity [1, 2]. Typically employed millisecond light pulses induce synchronous neuronal firing across a large population of neurons resembling discharges observed in diseased brains, e. g. during epileptic seizures [3]. Consequently, it is surprising that little effort has been made to extend optogenetic stimulation protocols beyond sequences of light pulses [4, 5]. Alternative stimulation patterns such as oscillating or randomly fluctuating light intensities [6] may further advance investigation of physiological processes. Of particular interest are stimulation paradigms that induce or modulate neuronal network oscillations [7, 8, 9]. These oscillations typically range between 1 – 130 Hz in both, humans and animal models [10] and are essential to subthreshold modulation of firing probabilities [11], modulation of plasticity [12], and to spatial coding [13]. To date, only a few studies described the effects of sinusoidal optical stimulation of excitatory neurons expressing channelrhodopsin 2 (ChR2), a blue-light sensitive opsin. These studies have shown the feasibility of ChR2-expressing neurons to follow a sinusoidal light input [4], drive cortical [6, 14] or subcortical [15, 16] local field potential (LFP) oscillations at a specific frequency, and entrain neuronal firing [17]. So far, *in vivo* evaluation of effects of sinusoidal stimulation on neural activity was limited to individual frequencies, and a systematic analysis of the full range of physiologically relevant frequencies is pending. The ability to manipulate these rhythms may permit studies of their neurophysiological function, and development of paradigms to intercept pathological oscillatory states [18, 19, 20, 21].

To monitor the effects of sinusoidal optical stimulation, delivery of light has to be accompanied by electrophysiological recordings. Combining these two functions in a single device reduces invasiveness while ensuring co-localization of recording and stimulation. It also, however, introduces interference between optically induced artifacts (e.g. Becquerel effects) and electrophysiological activity. Thermal drawing process, commonly used in optical fiber production, has recently enabled straightforward integration of optical waveguides with conductive electrodes [22, 23, 24]. These fiber-based devices employed

carbon-doped conductive polymer composites as electrode materials because of the similarity in their melting temperature (T_m) to the glass transition temperature (T_g) of transparent polymers constituting the waveguide core and cladding. The relatively low conductivity of polymer composites restricted the electrode dimensions to tens of microns to avoid large impedances unsuitable for extracellular recording *in vivo*. Electrodes composed of low T_m , such as tin, can be thermally drawn down to the dimensions of individual neurons ($<10\text{ }\mu\text{m}$), but require a polymer cladding with T_g close to their melting temperature (for tin $T_m = 232\text{ }^\circ\text{C}$) [23]. The latter, however, exhibit absorption and fluorescence in the visible part of the optical spectrum [25], which makes these polymers not suitable for light delivery. One way to enable scalable, high-resolution recording and optical neuromodulation is to combine these two materials systems within a single hybrid structure. Here, the utility of this approach is illustrated by integrating a low- T_g transparent polymer optical fiber into a hollow channel of a high- T_g polymer fiber incorporating 9 tin electrodes arranged around the channel. Low cross sectional area of the electrodes and their vertical alignment with the waveguide tip minimized the metal surface exposed to light and thereby the induced photo-electrochemical Becquerel effects [26], a feature of particular importance for continuous light stimulation with low modulation frequencies.

We implanted these hybrid fiber probes into the hippocampus (HC) of Thy1-ChR2-YFP transgenic mice [27], broadly expressing ChR2 predominantly in excitatory neurons [28], and compared hippocampal network responses to sinusoidal and pulsed light stimulation with various frequencies. The HC provides a convenient test bed for neuronal oscillations because it exhibits intrinsic oscillatory activity covering the full range of frequencies found in the mammalian brain [7]. Our findings corroborate the utility of the hybrid fiber-based probes for optogenetic modulation of LFP activity using sinusoidal and pulsed paradigms. Furthermore, we found the sinusoidal stimulation efficiency and recording quality remain stable over time, which confirms the utility of this combination of stimulation protocol and recording hardware for chronic, long-term applications. These observations may open research directions requiring precise control over network oscillations of differing frequencies, phases, and across brain areas [10].

2. Methods

2.1. Hybrid fiber probe fabrication

To integrate multichannel electrophysiological recording with optical neuromodulation in a flexible and miniature form factor, we combined previously described polymer-metal [23] and all-polymer fiber based probe designs [22]. Fiber drawing was employed to produce both, the fiber probe comprising 9 tin (Sn) electrodes encapsulated in polyetherimide (PEI) and a flexible waveguide with a polycarbonate (PC) core and cyclic olefin copolymer (COC) cladding. A PEI-Sn electrode array was produced by two consecutive thermal drawing steps as described previously [23]. In brief, a Sn rod (Puratronic rods, Alfa Aesar) with a diameter of 6 mm was inserted into a hollow PEI cylinder (McMaster-Carr, outer diameter 38.1 mm, inner diameter 6.4 mm). The resulting preform was thermally drawn at a temperature of $325\text{ }^\circ\text{C}$ and speed $0.1 - 0.2\text{ m/min}$ to produce a single-electrode fiber with an outer diameter of $2 - 3\text{ mm}$, and electrode diameter of $0.3 - 0.4\text{ mm}$. Nine 12 cm long sections of the

resulting fiber were incorporated into a PEI ring surrounded by a layer of PEI cladding. The structure was annealed at 253 °C for 15 min, and a polyphenylsulphone (PPSU, McMaster-Carr) sacrificial shell was added to improve the stability of the drawing process. This second-step preform was then drawn at a temperature of 300 °C and a speed of 0.85 m/min. The sacrificial PPSU shell was removed from the resulting fiber using tetrahydrofuran to produce a thinner probe with 470 µm outer diameter, electrode diameter of 9.6 µm, and hollow core with a diameter of 200 µm. Tin was selected as a material for the recording electrodes because of its high conductivity (8.7 MS/m) and the similarity of its melting temperature ($T_m = 232$ °C) to the glass transition temperature of PEI ($T_g = 215$ °C), a prerequisite for simultaneous thermal drawing of multiple materials.

A miniature PC-COC waveguide (75 µm outer diameter, 65 µm core diameter) was similarly produced by fiber drawing of a preform consisting of a PC core (McMaster-Carr, diameter of 4.8 mm), COC cladding (TOPAS, 0.8 mm thick) and a PC sacrificial shell (12.7 mm thick). The preform was annealed at 190 °C for 20 min, and the drawing was performed at a temperature of 250 °C and speed of 2.8 m/min. The PC shell was removed after the drawing using dichloromethane.

To produce a hybrid optoelectronic probe, the tin electrodes were exposed (>2 mm) on one end of the fiber by etching the PEI cladding using oxygen plasma (Glow Research, 100 W, 0.5 Torr, 60 min). The PC-COC fiber was attached to a zirconia ferrule (10.5 mm long, 2.5 mm in diameter, Thorlabs) to establish optical connection, and then inserted into the hollow core of the electrode array fiber. The electrodes were connected to contact pads on a printed circuit board (PCB, produced by Advanced Circuits using a custom layout) using conductive silver paint (Electron Microscopy Sciences). The probe, including the waveguide, was affixed to the PCB using 5 minute epoxy (VWR).

2.2. Probe Characterization

Cross-sectional images of the fiber probes were obtained by embedding them in resin matrix (Technovit 7100, Kulzer) and then cutting them using a microtome (Ultracut E, Reichert-Jung). Images were collected using an inverted optical microscope (AmScope) with a 20× objective.

Electrode impedance was measured by dipping the probe into saline solution (0.9 wt. %NaCl in water) along with a stainless steel reference wire (Goodfellow Cambridge Ltd.) and connecting them to an impedance analyzer (nanoZ, White Matter LLC). Impedance spectra for each electrode were collected for a frequency range between 10 – 4000 Hz. Furthermore, probes ($n = 2$) were tested in this saline bath for susceptibility to optical artifacts. An LED was coupled to the probe and light transmitted through the incorporated waveguide. Simultaneously, potential changes were recorded using the embedded electrodes. For this experiment, all 9 electrodes were shorted together, and pulsed and sinusoidal light stimulation with frequencies of 10 and 100 Hz was evaluated.

Optical transmission losses for the PC-COC fibers were determined by coupling these devices to a laser source (OEM Laser Systems, 50 mW maximum power, 473 nm wavelength) and measuring the transmitted optical power using a calibrated photodiode

(Newport, 918D-SL-0D1R). The measurement was repeated for multiple lengths for each waveguide ($n = 5$), and the transmitted power for each length was normalized to the power transmitted by the fiber cut directly at the ferrule tip to account for coupling losses.

2.3. In vivo electrophysiology

All animal procedures were approved by the MIT Committee on Animal Care. We employed male and female Thy1-ChR2-YFP mice (9 – 10 weeks old, line 18 [27, 28], generously donated by G. Feng, $n = 5$ or obtained from The Jackson Laboratories, $n = 2$) and a wild type mouse (C57Bl/6, 8 weeks old, The Jackson Laboratories, $n = 1$) housed at the MIT central animal facilities in 12 hour light/dark cycle at 22 °C with food and water *ad libitum*. Implantation surgeries were performed on deeply anesthetized mice (intraperitoneal injection, in mg/kg bodyweight: ketamine, 100; xylazine, 10; in saline), which were positioned in a stereotactic frame (David Kopf Instruments). Probes were connected using a 32-channel ZIF-clip connector to a headstage (PZ2–32, Tucker Davis Technologies Inc.) and digital system processor (RZ5D, TDT).

Probes were positioned in the hippocampal formation (coordinates from bregma [mm]: rostrocaudal (RC), -2 ; mediolateral (ML), -1.5 ; dorsoventral (DV), -1.9). In one Thy1-mouse a probe was first inserted to the right and subsequently into the left hippocampus (same RC and DV coordinates, but ML $+1.5$ mm). Recordings under acute anesthetized conditions were performed with a steel wire in the neck used as a reference. In mice that were implanted chronically, a steel reference and ground wire was attached to a skull screw positioned above the cerebellum. The probes were fixed to the skull using dental acrylic (Metabond, Parkell, followed by Jet-Set 4, Lang Dental). Following implantation surgeries, mice were returned to their home cages for recovery.

For light stimulation we used a diode-pumped solid-state (DPSS) laser (OEM Laser Systems, 50 mW maximum power, 473 nm wavelength) or a fiber-coupled light emitting diode (Plexon, PlexBright, 24.9 mW maximum power, 465 nm peak wavelength).

Light stimulation paradigms were programmed and controlled using the RZ5D digital processor. During recording, signals were filtered at 1 – 1000 Hz to identify LFPs and digitized at 12 kHz sampling frequency.

We tested pulsed and sinusoidal light stimulation paradigms with frequencies of 3, 5, 8, 10, 12, 16, 32, 70, 100, and 128 Hz. All tested stimulation frequencies were randomized within each pulse shape. Each trial contained stimulation blocks of 5 s spaced by 5 s rest epochs. For pulsed stimulation 5 ms pulse width was used at all frequencies. In addition, different pulse length (5 ms, 20 ms, 50 ms, at 10 Hz) were tested and response delays evaluated to corroborate the neural origin of the recorded potentials. Sinusoidal modulation of the light was accomplished by an analog modulation of the power input to the laser or LED and, in case of the laser, manually limiting the maximal output power to 35 mW. Stimulation was performed with 1 s ramp up and down to maximal light intensity, with 3 – 4 s illumination at maximal intensity ($1.9 - 64.0 \text{ mW/mm}^2$) to avoid transients due to the envelope of the sinusoidal stimulation. We confirmed the sinusoidal modulation of the light intensities at the

correct frequency by measuring the light output through a photodetector. Spectra of the measured light output showed a clear peak in the stimulation frequency.

While LEDs produced stable light intensities over cycles, laser light intensity did not reach maximum in some cycles. To detect those cycles and identify the actual light intensity, 5% of the laser light was redirected into a photodetector using a glass beamsplitter.

To corroborate neuronal origin of stimulation responses we measured changes in potential in response to pulsed and sinusoidal light (LED) stimulation with a fiber dipped into saline and acutely implanted into the HC of an anesthetized Thy1-ChR2-YFP mouse, which was then euthanized during the measurement. The mouse remained connected to the experimental setup while it was injected with a euthanasia solution (Fatal Plus intraperitoneal injection, 100 mg/kg bodyweight) and the full set of frequencies and patterns were tested again ~300 s after respiration had stopped. Stimulation in the euthanized mouse started with sinusoidal patterns followed by all pulsed patterns, both protocols lasting for ~30 min. Furthermore, one WT mouse was acutely implanted, and pulsed light stimulation (5 ms, 10 and 100 Hz) was applied.

2.4. Data Analysis

All data were analyzed using custom algorithms written in Matlab (Mathworks, R2014a). For the settings applied in this study, no differences in electrophysiological response (amplitudes and power spectra) to the laser and LED light sources were found and therefore data were pooled.

LFP response to stimulation was measured as deviation of the amplitude from the baseline (z-scored by subtracting the mean and normalizing to the standard deviation of LFPs during inter-stimulus intervals, 'light_{OFF}') and averaged over stimulation blocks and cycles. We applied bandstop filtering (2nd order Butterworth, 58 – 62 Hz) to eliminate 60 Hz noise from individual recordings. To estimate stimulation effectiveness, only cycles with peak light intensities >80% of maximum light intensity were considered (ramp up/down periods or laser power break downs excluded).

Square pulse and sinusoidal stimulation patterns were compared at 10 Hz and 100 Hz in mice acutely implanted with hybrid fiber probes. For both frequencies, the response peak per cycle was identified in the z-scored LFP, and peak amplitudes were averaged over cycles and stimulation blocks ($n_{blocks} = 9$) in each animal ($n_{animal} = 5$, $n_{implantations} = 6$). In four recordings, sinusoidal stimulation at 10 Hz was not tested, and therefore LFP peak amplitudes were interpolated from 8 Hz and 12 Hz stimulation responses. To account for differences across animals and different light power across implants, all stimulation responses (pulsed/sinusoidal, 10/100 Hz) were normalized to the mean peak amplitude in response to 10 Hz pulse stimulation in each animal.

To validate the neuronal origin of stimulation responses we measured changes in potential with the probes dipped into saline, inserted into the HC of an alive Thy1-ChR2-YFP mouse, and in the same mouse minutes after euthanasia. We compared average response amplitudes (filtered: 2nd order Butterworth, bandstop 58 – 62 Hz) to pulsed and sinusoidal stimulation

(5 – 128 Hz) for both conditions and computed spectrograms and spectra of the median block response (17 blocks, 2 – 500 Hz, 0.5 s window, 100 ms overlap) and estimated the power difference at the stimulation frequency between both conditions.

Coherence and cross-spectral phase angles were calculated between z-scored LFP and light stimulation (laser and LED, waveforms over the full 5 s stimulation block including light intensity ramps and fluctuations in laser power) to characterize the entrainment of the neuronal response by the sinusoidal light stimulation. All cycles were included to investigate whether neural response intensity varied proportionally to the light power density. Since intracellular depolarization due to light-gated ChR2-mediated cation influx results in a negative extracellularly measured LFP, we inverted the LFP signals before we estimated cross-spectral phase angles and delays. Coherence and phase angles were calculated for every stimulation frequency in each stimulation block and averaged across blocks ($n_{blocks} = 9$) for each experiment ($n_{animal} = 5$, $n_{implantation} = 6$). To differentiate between neuronal response and light artifacts we calculated the difference between these phase angles in the living and subsequently euthanized Thy1-ChR2-YFP mouse.

To assess long-term stability of the observed optically evoked responses, recordings were performed over a period of up to 55 days following implantation ($n_{animal} = 2$). Collected LFP responses to optical stimulation were offset by subtracting mean LFPs obtained during light_{OFF} epochs. Maximal LFP amplitudes within 125 ms (8 Hz sinusoidal) or 100 ms (10 Hz pulsed) stimulation cycles were detected. The median LFP peak amplitude across stimulation cycles and blocks was calculated and normalized to the maximal light input (all chronic recordings were performed with LED light sources, light input into the probe was measured for each experiment). Coherence and phase angle between LFP and sinusoidal light input were calculated for all time points.

3. Results

3.1. Hybrid Fiber Probe

To produce a probe combining multi-site electrophysiological recording and optical stimulation we employed thermal drawing process. While it is possible to combine optical waveguides and conductive electrodes within fully integrated fibers, the low T_g values of optically-transparent polymers needed for waveguide designs have, so far, limited the electrode materials to conductive polymer composites. The low conductivity of the latter, in turn, resulted in electrode dimensions of tens of microns to achieve impedance values in the range useful for recording of isolated single neuron spikes and LFPs ($<1\text{ M}\Omega$ at 1 kHz) [29, 30]. To overcome this limitation, two-component fiber probes comprising a hollow core (inner diameter 200 μm , outer diameter 470 μm) array of 9 tin electrodes with diameters of $9.6 \pm 2.1\text{ }\mu\text{m}$ (mean \pm standard deviation) embedded in PEI cladding and a transparent optical fiber with a PC core and COC cladding (core diameter 65 μm , outer diameter 75 μm) were fabricated. In these probes, the polymer optical fibers were inserted into the hollow channels of the electrode arrays (Fig. 1A). The fully assembled devices, including a printed circuit board (PCB) for electrical connection to the electrophysiology setup and a ferrule for connection to the light sources weighted $0.457 \pm 0.003\text{ g}$ (mean \pm standard deviation, $n_{samples} = 3$), allowing for their chronic implantation into adult mice without observable

decrease in their mobility (Supplementary Fig. S1). The impedance of tin microelectrodes was $627 \pm 225 \text{ k}\Omega$ at 1 kHz (mean \pm std, $n = 6$, Fig. 1B), which is suitable for simultaneous recording of low frequency LFPs and high frequency spikes [31].

Optical fibers with a PC core (refractive index $n = 1.58$) and COC cladding ($n = 1.52$) were capable of transmitting 473 nm light with a loss of 2.44 dB/cm, which is comparable to previously reported values for this materials combination (Fig. 1C, [22]).

3.2. Combined electrophysiological recordings and optical stimulation

To test the utility of the hybrid fibers for combined optogenetic stimulation and electrophysiological recording, we acutely inserted and/or implanted these probes into the HC of transgenic Thy1-ChR2-YFP and wild-type mice, and recorded spontaneous electrophysiological activity both in anesthetized and awake animals. We chose Thy1-ChR2-YFP mice line 18 [27] to ensure strong expression of ChR2 in the majority of hippocampal excitatory cells [28]. Recordings of hippocampal LFPs (Fig. 1D), which were dominated by characteristic theta (5 – 12 Hz) and gamma (30 – 90 Hz) frequency oscillations (Fig. 1E), corroborated the ability of the hybrid fiber probes to record both types of neural signals.

Next, we tested whether light transmitted through the incorporated waveguide was sufficient to optically evoke neuronal responses. We first acutely inserted the fiber-based probes into the HC of Thy1-ChR2-YFP mice and applied light pulses of varying length (Fig. 1F; 5, 20, 50 ms, 10 Hz, $n_{\text{pulses}} = 18$, first pulse per block). Pulses lasting 5 ms induced negative LFP peaks that reached their minimum after the pulses ended (amplitude peaked at $-0.35 \pm 0.02 \text{ mV}$ after $5.6 \pm 0.5 \text{ ms}$) and thereby underline the neuronal origin of the recorded potentials. Longer pulses resulted in only marginally larger amplitudes (20 ms: $-0.37 \pm 0.02 \text{ mV}$; 50 ms: $-0.37 \pm 0.02 \text{ mV}$; one-way ANOVA $p = 0.03$; pairwise Tukey's test reaching Significance only for $p_{5\text{ms}/20\text{ms}} < 0.05$), but the time until minimum scaled with the length of the pulses (20 ms: $11.4 \pm 3.7 \text{ ms}$; 50 ms: $17.0 \pm 5.8 \text{ ms}$; one-way ANOVA $p < 0.001$; all pairwise comparisons $p < 0.005$). This is consistent with the results from intracellular recordings showing a dependence of the delay on the light pulse duration and a saturation of the maximum current for pulses longer than 10 ms [32].

To further prove that the recorded signals are caused by light-gated ChR2 currents, we consecutively implanted a fiber-probe into the HC of a Thy1-ChR2-YFP and WT mouse and applied identical pulsed optical stimulation protocol (5 ms at 10 and 100 Hz). Stimulation induced correlated LFP deflections in the Thy1-ChR2-YFP mouse but not in the WT mouse (Supplementary Fig. S2). Analogous, there was a pronounced spectral in the spectrum of the LFP at the stimulation frequency when stimulating Thy1-ChR2-YFP mice that was absent in WT mice. This confirmed the solely neuronal origin of the observed signals in response to pulsed stimulation in Thy1-ChR2-YFP mice.

3.3. Comparison of sinusoidal and pulsed optical stimulation

The ability to manipulate naturally occurring oscillatory potentials that synchronously influence the excitability of large neuronal populations would permit studies of generation and function of these rhythms and pathologies associated with them. Despite technological advances in optogenetics and optoelectronics that enable simultaneous recording and

stimulation with pulsed light [33, 34], alternative neuromodulation protocols have received limited attention. Here we applied the hybrid fiber probes to investigate electrophysiological responses to sinusoidally modulated light with frequencies covering the entire range of hippocampal rhythms and compared them to those evoked by pulsed stimulation.

We recorded responses to both stimulation paradigms on all connectorized electrodes (Supplementary Fig. S3). The response amplitudes varied across electrodes and this variation was correlated with the impedance of the electrodes (correlation coefficient_{pulsed} = 0.98; correlation coefficient_{sin} = 0.95). To estimate the effectiveness of the stimulation we used the recording channels with the highest signal-to-noise ratios for further analyses.

Trains of short light pulses (5 ms pulse width, 3, 5, 8, 10, 12, 16, 32, 70, 100, and 128 Hz, wavelength 473 nm) delivered through a hybrid probe into the HC of Thy1-ChR2-YFP mice led to immediate significant deflections in the LFP exceeding the variance of the baseline fluctuations for all frequencies tested (Fig. 2A, significantly different amplitude distribution between light ON and OFF periods, $p_{OFF/ON} < 0.001$). Even for high pulse rates the LFP reflected individual stimulus cycles but responses were of smaller amplitudes than the amplitudes seen for lower frequencies (Fig. 2B).

Sinusoidal stimulation evoked sinusoidal patterns in the LFP at all frequencies tested (Fig. 2C, amplitude distribution $p_{OFF/ON} < 0.001$) that were clearly different from responses to pulsed stimulation. LFP responses to sinusoidal stimulation had smaller amplitudes but similarly reliably followed the stimulation even at high frequencies (Fig. 2D). Note, that the LFP response is inverted to the light input. This is expected since an intracellular depolarization due to light-gated ChR2-mediated cation influx results in a negative extracellularly measured LFP signal.

We compared the LFP response amplitudes of pulsed and sinusoidal stimulation at 10 Hz and 100 Hz (Fig. 2E; $n_{animals} = 5$, $n_{fibers} = 4$, $n_{cycles} = 80$, 2-way ANOVA showing significant difference across stimulation frequencies and patterns, $p_{parameters} < 0.001$, $p_{interactions} < 0.001$, all pairwise comparisons $p < 0.005$). Responses to sinusoidal stimulation at 10 Hz were $55.44 \pm 30.54\%$ lower than to 10 Hz pulsed (5 ms) stimulation (*post hoc* comparison, $p < 0.001$). Stimulation with a 100 Hz pulse elicited amplitude peaks $28.27 \pm 23.01\%$ and 100 Hz sinusoidal stimulation $14.10 \pm 10.97\%$ of those obtained with 10 Hz pulsed stimulation, with responses to 100 Hz sinusoidal stimulation being significantly lower than those to pulsed stimulation ($p < 0.001$). For both stimulation paradigms, response amplitudes decreased significantly from 10 Hz to 100 Hz. Note that at 10 Hz for the same peak intensity the energy delivered per sinusoidal stimulation cycle is 10 times larger than the energy delivered by a single 5 ms pulse (5% duty cycle). In contrast, at 100 Hz the delivered energies are matched for the stimulation paradigms (50% duty cycle for pulses).

Given these strong differences between both patterns and frequencies we tested the neuronal origin of the signals before further characterizing the response to sinusoidal light stimulation. Metal electrodes employed for electrophysiology are commonly susceptible to optical artifacts and photo-electrochemical effects are known to scale with light intensity and electrode surface [26]. Thus, our hybrid probes incorporating small electrodes vertically

aligned with the light emission plane (fiber tip) should, in principle, minimize those artifacts. This is essential to sinusoidal stimulation paradigms with slow modulation frequencies since electrodes are permanently illuminated, and the absolute amount of light per cycle is higher than that delivered by 5 ms pulses.

We first examined our probes for optical artifacts by running the stimulation protocol while the probes were immersed in a saline bath. Apart from a small spectral peak at 100 Hz during pulsed stimulation at 100 Hz, there were no potential changes in response to the stimulation (Fig. 3I–L). Since the scattering properties of brain tissue differ from those of a saline solution, and light is more likely to be reflected and scattered onto the electrode surfaces *in vivo*, we tested the neuronal nature of the observed LFP responses by implanting a probe into the HC of an anesthetized Thy1-ChR2-YFP mouse which was subsequently euthanized. We applied pulsed (5 ms pulse width) and sinusoidal stimulation in the living animal and repeated the stimulation 5 minutes following termination of respiration. The LFP response in the living animal followed the stimulation pattern for both stimulation paradigms, resulting in a prominent spectral peak confined to the stimulation frequency (Fig. 3A–D, Supplementary Fig. S4,5). After euthanizing the animal, the spectral peaks in response to pulsed stimulation were mostly absent (Fig. 3E,F). Remaining peaks were negligibly small and, for the 100 Hz stimulation, identical to that seen in the saline test (Fig. 3M,N). Sinusoidal stimulation in the dead mouse, however, evoked small oscillatory potentials (e.g. 57 μ V for 10 Hz, Fig. 3G; 5 μ V for 100 Hz, Fig. 3H). Nevertheless, these signals were much smaller for all frequencies than the LFP responses observed in the living animal (e.g. 463 μ V for 10 Hz, Fig. 3C; 52 μ V for 100 Hz, Fig. 3D; for all frequencies $\delta_{power} = -34.54 \pm 9.39$ dB) and, in particular at the lower frequencies, did no longer show the characteristic anti-correlation between light input and LFP response observed in living mice (Supplementary Fig. S5). Thus, even though we found negligible oscillatory potentials in the euthanized animal, they differed both in magnitude and phase from the LFP responses observed in the living animals.

Our data indicate that a broad range of sinusoidal stimulation frequencies can induce oscillatory patterns in the LFP that predominantly originate from neuronal sources. Amplitudes of responses to sinusoidal stimulation are smaller than those resulting from pulsed paradigms and decrease with increasing stimulation frequency.

3.4. Coherent entrainment of LFPs by sinusoidal stimulation

We further explored the functional form of the amplitude decay observed over frequency and therefore compared response amplitudes evoked by sinusoidally modulated stimulation at 3, 5, 8, 10, 12, 16, 32, 70, 100, and 128 Hz. Indeed, amplitudes of optically evoked LFP oscillations decreased with increasing frequency, and this decay could be fitted by a logarithmic function (Fig. 4A). Note that at stimulation frequencies of 70 Hz or higher oscillatory patterns were recognizable as rhythmic patterns in the ongoing LFP as well as in the averaged cycle responses (Fig. 2D) and as peaks in the spectrogram confined to the stimulation frequency (Supplementary Fig. 5) but amplitudes were only as large as the standard deviation of the LFP during light_{OFF} periods.

To validate whether the observed amplitude decay results from the decline in energy per cycle due to the shortening of stimulation cycles with increasing frequencies, we estimated the total energy delivered to the tissue through all hybrid fibers in these experiments. The energy per cycle for increasing frequencies followed a reciprocal linear function (Fig. 4A). Thus, the exponential decay found in LFP response amplitudes was not purely reflecting the reduction in delivered energy for increasing frequencies.

To study or manipulate intrinsic network rhythms it is essential to induce coherent oscillations with a reliable phase delay with respect to the sinusoidal light input. We, therefore, analyzed coherence between optical stimuli and LFP response (Fig. 4B–C; $n_{\text{animals}} = 5$, $n_{\text{fibers}} = 4$, $n_{\text{cycles}} = 80$). LFP oscillations evoked by sinusoidal stimulation were coherent with light input even at high frequencies where amplitudes were small (Fig. 4C; mean coherence = 0.88 ± 0.06), being lowest at 3 Hz (0.78 ± 0.17) and highest at 12 Hz (0.93 ± 0.06). Cross-spectral phase delays between peak light intensity and the trough of the LFP amplitude increased over frequencies up to 32 Hz (Fig. 4D, circular correlation coefficient = 0.85, $p < 0.0001$; circular statistics toolbox for Matlab [35]). At frequencies of 70 Hz and higher, where response amplitudes were close to background fluctuations, phase delays were variable across animals. Consequently, in some animals, the LFP was no longer phase-inverted with respect to the optical stimulus. Furthermore, when comparing the cross-spectral phase angles between light and LFP response obtained from the living and dead Thy1-ChR2-YFP mouse, the difference between both angles became small for frequencies at 70 Hz or higher (Supplementary Fig. S5). Nevertheless, the power peaks were considerably larger in the living animal than postmortem. Thus, we concluded that the signals obtained at frequencies of 70 Hz or higher are better understood as being a mixture of optical artifacts and neuronal response. Interestingly, these frequencies are equal or larger than the cutoff frequency of ChR2 (69 Hz, [4]).

For the lower frequencies (< 12 Hz), when cross-spectral phase delays were converted into time domain (Supplementary Fig. S6A), it became apparent that the peak response in some animals occurred on the increasing flank of the light oscillation. This was caused by skewed LFP responses resulting from gamma band oscillations superimposed onto the slow oscillation correlated with stimulation (Supplementary Fig. S6B–C, [15]). To obtain a more precise estimate of the delay between light and slow LFP oscillations we computed the latency between the time point when the light was off and the time of the smallest LFP deflection for all frequencies up to 32 Hz. This minimized the influence of the superimposed gamma oscillation onto the latency estimate. The LFP response followed the optical stimulus with a latency stable across frequencies and animals (Fig. 4E, mean temporal delay = 8.16 ± 5.33 ms, correlation coefficient = -0.16 , $p = 0.35$, $n_{\text{blocks}} = 9$). Thus, we were able to overwrite ongoing hippocampal activity by light induced LFP rhythms that were coherent with the light input. Phase and time lags could be only reliably estimated for frequencies below the cutoff frequency set by ChR2 kinetics. Consequently, amplitude and phase delay of the induced oscillation are dependent on the stimulation frequency and, at lower frequencies, on the initiation of nested gamma oscillations.

3.5. Reliability of optically evoked responses

For behavioral studies, it is desirable that the probes and the stimulation patterns retain their functions over extended periods of time following implantation. Therefore, we chronically implanted the developed hybrid fiber probes into the HC of Thy1-ChR2-YFP mice and recorded LFP responses to optical stimulation over 55 days. Sinusoidal stimulation at 8 Hz evoked large and coherent LFP responses immediately following probe insertion (Fig. 5A, day 0), and the effects persisted over a 55-day period (Fig. 5A,B). The average LFP amplitude evoked by sinusoidal stimulation (peak power density $3.12 \pm 1.27 \text{ mW/mm}^2$, mean \pm std) was $-0.20 \pm 0.11 \text{ mV}$ ($n_{\text{animals}} = 2$, $n_{\text{cycles}} = 570$ per day). To assess the efficacy of stimulation over time we normalized the LFP response amplitude to the stimulation intensity amplitude and found an average responsiveness of $-0.08 \pm 0.05 \text{ mV} \times \text{mm}^2/\text{mW}$. The responsiveness of the tissue did not change significantly over time (Fig. 5C, correlation coefficient = 0.33, $p = 0.34$). We also validated the stability of the electrophysiological responses elicited by 5 ms light pulses at a frequency of 10 Hz. Akin to the sinusoidal stimulation, pulsed stimulation evoked reliable LFP responses (Fig. 5D, average amplitude = $-0.55 \pm 0.27 \text{ mV}$, $n_{\text{cycles}} = 270$) over the entire 55 day period, and efficacy of the stimulation remained stable over time (Fig. 5E, correlation coefficient = 0.02, $p = 0.98$).

In addition to stable response amplitudes, high coherence and a constant phase delay between the light input and the LFP response are desirable. The coherence between the 8 Hz sinusoidal light input and LFP readout at the stimulation frequency was stable (Fig. 5F, correlation coefficient = -0.25 , $p = 0.56$, $n_{\text{blocks}} = 20$ per day) and ranged between 0.88 – 0.97 over the entire 55 day period. The phase angle between light input and LFP oscillation fluctuated at $28.51^\circ \pm 5.11^\circ$ with no significant dependence on implantation duration (Fig. 5G, circular correlation coefficient = 0.67, $p = 0.13$) and was in the range of values obtained in acute experiments (Fig. 4C, $16.95^\circ \pm 14.61^\circ$). Stability of LFP response amplitudes, phase angles, and coherence values with respect to sinusoidal stimulation over the period of 55 days indicates the reliability of the stimulation paradigm, and the chronic utility of the optoelectronic fiber probes.

4. Discussion

In this study, we investigated the effect of sinusoidal optical stimulation on hippocampal LFPs in transgenic Thy1-ChR2-YFP mice. For this purpose we designed a hybrid fiber probe capable of delivering light and recording LFP simultaneously. While pulsed optical stimulation is commonplace in neuroscience experiments that rely on optogenetics, the applications of sinusoidally modulated light remained limited despite its potential to elicit or entrain network oscillations underlying neurophysiological processes such as memory formation and consolidation [13].

Stimulation with continuously modulated light at low frequencies implies a permanent, and therefore high-energy, illumination of metal recording electrodes placed directly within in the light cone. Thus, pairing sinusoidal stimulation with electrophysiological recording demands probes with minimal photo-electrochemical artifacts. We employed fiber drawing to fabricate such hybrid probes comprising a hollow core array of 9 tin electrodes (each $9.6 \mu\text{m}$ in diameter) embedded in a PEI cladding and a $75 \mu\text{m}$ PC-COC optical fiber integrated

into the array core. Optical artifacts [36, 37] observed for metal electrodes scale with surface area and light power [26]. By integrating tin electrodes with small surface areas vertically aligned with the waveguide tip, and predominantly outside the light cone, these probes were designed to minimize optical artifacts, such as Becquerel effects. In line with this hypothesis artifacts during pulsed stimulation were negligibly small. Sinusoidal stimulation, however, produced oscillating potentials in HC 5 minutes following euthanasia of a Thy1-ChR2-YFP mouse. Nevertheless, these oscillations were ~35 dB smaller in power, and, in particular at lower frequencies, lacked the typical phase inversion between LFP and optical stimulus observed for all live mice at these frequencies.

Probes integrating tin electrodes have been previously shown to be biocompatible *in vivo* [23, 38] and their impedance lies within the range suitable for extracellular recordings [29, 30]. Furthermore, our hybrid structures combining a cylindrical PEI-electrode array and a PC-COC waveguide may potentially overcome the scaling challenges faced by all-polymer devices, where the degree of miniaturization and, consequently, the density of the recording electrodes is limited by the relatively low conductivity (10^4 S/m) of polymer-carbon composites [39]. Consistent with prior work, the incorporated PC-COC optical fibers are capable of delivering light with power densities sufficient for use in optogenetic experiments (>1 mW/mm²) with the input provided by common lasers and LEDs, albeit with higher losses (2.44 dB/cm) than conventional silica fibers (<0.0002 dB/cm). Finally, the flexibility of these polymer fibers facilitates their back-end connection and integration with the interface electronics used for recording.

We applied our hybrid fiber-based probes to investigate the capability of sinusoidal light stimulation to induce hippocampal LFP oscillations across a broad range of physiologically relevant frequencies. Sinusoidal optical stimulation has been previously employed to induce rhythmic currents and firing in single neurons [4, 17] or to drive neuronal populations [6, 14, 15, 16]. Prior studies that investigated electrophysiological effects of sinusoidal stimulation *in vivo* were limited to a single frequency. We extended these analyses to the full range of physiological frequencies in the HC (3 – 128 Hz). Both optical stimulation patterns, sinusoidal and pulsed, evoked neural population responses across the entire frequency range, with the LFP amplitude decreasing at higher stimulation frequencies. For pulsed stimulation our observations *in vivo* were consistent with effects described by Mattis et al. for firing of individual neurons *in vitro* [40]. The likelihood to induce a spike decreases with higher frequencies. That is reflected by a smaller amplitude in the LFP response. Similarly, we attribute the observed logarithmic decay in amplitude over frequency in response to sinusoidal stimulation to ChR2 channel kinetics [32] and to the frequency adaption of individual neurons [41, 42, 27] rather than to the linear reduction in optical power density.

Despite this decrease in amplitude the LFP followed stimulation frequencies up to 128 Hz, visible as a power peak at the stimulation frequency and as a high coherence between sinusoidal optical stimulus and neural response. An entrainment of hippocampal LFPs beyond 69 Hz, the cutoff frequency of ChR2 [4], however, raised questions about optical artifacts. The dramatic decrease of the frequency-specific power peak after euthanizing the mouse argues for neuronal activity as the predominant source of the observed oscillations at all frequencies. This is in agreement with reports showing that ChR2 has a sustained

conductance at 70 Hz [4] that is sufficient to induce sparse action potential firing [40]. On the contrary, phase lags between light input and LFP readout could be reliably determined only for frequencies of up to 32 Hz and considerably varied across animals at higher frequencies. Considering that at higher frequencies the anti-correlation between light input and LFP readout is lost and that the corresponding phase angles become more similar to those observed in a euthanized mouse, we consider signals resulting from sinusoidal stimulation at 70 Hz to comprise a mixture of optical artifacts and neuronal responses, which highlights the importance of thorough control experiments at these frequencies where the optical artifacts may considerably influence the electrophysiological measurement.

Another important factor that needs consideration when estimating phase or time delays are the superimposed indirectly induced gamma oscillations [14, 15]. All stimulation frequencies below gamma were capable of inducing a secondary gamma burst. The superposition of gamma oscillations further underlines the neuronal origin of the recorded signals at those frequencies. Overlapping gamma activity was coupled to the peak of the response and therefore led to skewed LFP sinusoids. Since skewed sinusoids result in imprecise cross-spectral phase angles we, instead, estimated the latencies between the minimum of the optical stimulus and the smallest LFP response and found that the latencies were comparable for all frequencies <70 Hz and in the range of delays found in response to brief light pulses [32].

Finally, optically-evoked responses to sinusoidal stimuli in Thy1-ChR2-YFP mice implanted with hybrid fiber probes in the HC were stable for up to 55 days. We found no significant change in the LFP amplitude response, coherence, and phase lag, during this period. This further supports previous findings indicating durability and biocompatibility of fibers composed of PEI, tin, PC and COC [23, 24].

In this study, we developed a toolkit to manipulate or induce network oscillations. This toolkit may enable investigation of the role of field potential oscillations in memory formation and consolidation, representation of respective position in space, as well as in pathologies such as epilepsy, Parkinson's disease and autism.

Supplementary Material

Refer to Web version on PubMed Central for supplementary material.

Acknowledgments

This work was supported by the National Institute of Neurological Disorders and Stroke (5R01NS086804), the Center for Sensorimotor Neural Engineering, a National Science Foundation (NSF) Engineering Research Center (EEC-1028725), NSF CAREER award to P.A. (CBET-1253890), NSF Center for Materials Science and Engineering (DMR-1419807, IRG-I), the US Army Research Laboratory and the US Army Research Office through the Institute for Soldier Nanotechnologies (W911NF-13-D-0001), by a grant from the Simons Foundation to the Simons Center for the Social Brain at MIT, the German Federal Ministry of Education and Research (FKZ 01GQ0830) and by the German Science Foundation within the Cluster of Excellence BrainLinks-BrainTools (EXC 1086).

References

1. Fenno L, Yizhar O, Deisseroth K. The Development and Application of Optogenetics. *Annual Review of Neuroscience*. 2011; 34:389–412. 7.
2. Deisseroth K. Optogenetics: 10 years of microbial opsins in neuroscience. *Nature neuroscience*. 2015; 18:1213–25. 9. [PubMed: 26308982]
3. Osawa S-Iwasaki M, Hosaka R, Matsuzaka Y, Tomita H, Ishizuka T, Sugano E, Okumura E, Yawo H, Nakasato N, Tominaga T, Mushiake H. Optogenetically Induced Seizure and the Longitudinal Hippocampal Network Dynamics. *PLoS ONE*. 2013; 8:e60928. 4. [PubMed: 23593349]
4. Tchumatchenko T, Newman JP, Fong M-f, Potter SM. Delivery of continuously-varying stimuli using channelrhodopsin-2. *Frontiers in neural circuits*. 2013; 7(December):184. [PubMed: 24367294]
5. Lignani G, Ferrea E, Difato F, Amarù J, Ferroni E, Lugarà E, Espinoza S, Gainetdinov RR, Baldelli P, Benfenati F. Long-term optical stimulation of channelrhodopsin-expressing neurons to study network plasticity. *Frontiers in molecular neuroscience*. 2013; 6(August):22. [PubMed: 23970852]
6. Newman JP, Fong M-f, Millard DC, Whitmire CJ, Stanley GB, Potter SM. Optogenetic feedback control of neural activity. *eLife*. 2015; 4(February 2016):e07192. [PubMed: 26140329]
7. Buzsáki G. *Rhythms of the Brain*. 2009
8. Colgin LL, Moser EI. Gamma oscillations in the hippocampus. *Physiology (Bethesda)*. 2010; 25(5): 319–329. [PubMed: 20940437]
9. Sullivan D, Mizuseki K, Sorigi A, Buzsaki G. Comparison of sleep spindles and theta oscillations in the hippocampus. *Journal of Neuroscience*. 2014; 34(2):662–674. [PubMed: 24403164]
10. Axmacher N, Henseler MM, Jensen O, Weinreich I, Elger CE, Fell J. Cross-frequency coupling supports multi-item working memory in the human hippocampus. *Proceedings of the National Academy of Sciences*. 2010; 107:3228–3233. 2.
11. Klausberger T, Somogyi P. Neuronal diversity and temporal dynamics: the unity of hippocampal circuit operations. *Science (New York, N.Y.)*. 2008; 321:53–7. 7.
12. Fell J, Axmacher N. The role of phase synchronization in memory processes. *Nature Reviews Neuroscience*. 2011; 12:105–118. 2. [PubMed: 21248789]
13. Buzsáki G, Moser EI. Memory, navigation and theta rhythm in the hippocampal-entorhinal system. *Nature neuroscience*. 2013; 16:130–8. 1. [PubMed: 23354386]
14. Pastoll H, Solanka L, van Rossum MCW, Nolan MF. Feedback Inhibition Enables Theta-Nested Gamma Oscillations and Grid Firing Fields. *Neuron*. 2013; 77(1):141–154. [PubMed: 23312522]
15. Butler JL, Mendonca PRF, Robinson HPC, Paulsen O. Intrinsic Cornu Ammonis Area 1 Theta-Nested Gamma Oscillations Induced by Optogenetic Theta Frequency Stimulation. *Journal of Neuroscience*. 2016; 36(15):4155–4169. [PubMed: 27076416]
16. Laxpati NG, Mahmoudi B, Gutekunst C-A, Newman JP, Zeller-Townson R, Gross RE. Real-time in vivo optogenetic neuromodulation and multielectrode electrophysiologic recording with NeuroRighter. *Frontiers in neuroengineering*. 2014; 7(October):40. [PubMed: 25404915]
17. Royer S, Zemelman BV, Barbic M, Losonczy A, Buzsáki G, Magee JC. Multi-array silicon probes with integrated optical fibers: light-assisted perturbation and recording of local neural circuits in the behaving animal. *European Journal of Neuroscience*. 2010; 31:2279–2291. 6. [PubMed: 20529127]
18. Froriep UP, Kumar A, Cosandier-Rimé D, Häussler U, Kilias A, Haas Ca, Egert U. Altered theta coupling between medial entorhinal cortex and dentate gyrus in temporal lobe epilepsy. *Epilepsia*. 2012; 53:1937–1947. 11. [PubMed: 22984867]
19. Lopez-Azcarate J, Tainta M, Rodriguez-Oroz MC, Valencia M, Gonzalez R, Guridi J, Iriarte J, Obeso JA, Artieda J, Alegre M. Coupling between beta and high-frequency activity in the human subthalamic nucleus may be a pathophysiological mechanism in Parkinson's disease. *J Neurosci*. 2010; 30(19):6667–6677. [PubMed: 20463229]
20. Ibarz JM, Foffani G, Cid E, Inostroza M, Menendez de la Prida LM. Emergent dynamics of fast ripples in the epileptic hippocampus. *The Journal of neuroscience: the official journal of the Society for Neuroscience*. 2010; 30(48):16249–16261. [PubMed: 21123571]

21. Kilias A, Häussler U, Heining K, Froriep UP, Haas CA, Egert U. Theta frequency decreases throughout the hippocampal formation in a focal epilepsy model. *Hippocampus*. 2018; 0(0)
22. Lu C, Froriep UP, Koppes RA, Canales A, Caggiano V, Selvidge J, Bizzi E, Anikeeva P. Polymer fiber probes enable optical control of spinal cord and muscle function in vivo. *Advanced Functional Materials*. 2014; 24(42):6594–6600.
23. Canales A, Jia X, Froriep UP, Koppes RA, Tringides CM, Selvidge J, Lu C, Hou C, Wei L, Fink Y, Anikeeva P. Multifunctional fibers for simultaneous optical, electrical and chemical interrogation of neural circuits in vivo. *Nature Biotechnology*. 2015; 33(3):277–284.
24. Park S, Guo Y, Jia X, Choe HK, Grena B, Kang J, Park J, Lu C, Canales A, Chen R, Yim YS, Choi GB, Fink Y, Anikeeva P. One-step optogenetics with multifunctional flexible polymer fibers. *Nature Neuroscience*. 2017; (June 2016)
25. Koppes RA, Park S, Hood T, Jia X, Abdolrahim Poorheravi N, Achyuta AH, Fink Y, Anikeeva P. Thermally drawn fibers as nerve guidance scaffolds. *Biomaterials*. 2016; 81:27–35. [PubMed: 26717246]
26. Kozai TDY, Vazquez AL. Photoelectric artefact from optogenetics and imaging on microelectrodes and bioelectronics: new challenges and opportunities. *Journal of Materials Chemistry B*. 2015; 3(25):4965–4978. [PubMed: 26167283]
27. Arenkiel BR, Peca J, Davison IG, Feliciano C, Deisseroth K, Augustine GJ, Ehlers MD, Feng G. In Vivo Light-Induced Activation of Neural Circuitry in Transgenic Mice Expressing Channelrhodopsin-2. *Neuron*. 2007; 54(2):205–218. [PubMed: 17442243]
28. Asrican B, Augustine GJ, Berglund K, Chen S, Chow N, Deisseroth K, Feng G, Gloss B, Hira R, Hoffmann C, Kasai H, Katarya M, Kim J, Kudolo J, Lee LM, Lo SQ, Mancuso J, Matsuzaki M, Nakajima R, Qiu L, Tan G, Tang Y, Ting JT, Tsuda S, Wen L, Zhang X, Zhao S. Next-generation transgenic mice for optogenetic analysis of neural circuits. *Frontiers in neural circuits*. 2013; 7(November):160. [PubMed: 24324405]
29. Ferguson JE, Boldt C, Redish AD. Creating low-impedance tetrodes by electroplating with additives. *Sensors and Actuators, A: Physical*. 2009; 156(2):388–393. [PubMed: 21379404]
30. Williams JC, Hippensteel JA, Dilgen J, Shain W, Kipke DR. Complex impedance spectroscopy for monitoring tissue responses to inserted neural implants. *J. Neural Eng.* 2007; 4:410–423. [PubMed: 18057508]
31. Nelson MJ, Pouget P, Nilsen EA, Patten CD, Schall JD. Review of signal distortion through metal microelectrode recording circuits and filters. *Journal of Neuroscience Methods*. 2008; 169(1):141–157. [PubMed: 18242715]
32. Nikolic K, Grossman N, Grubb MS, Burrone J, Toumazou C, Degenaar P. Photocycles of Channelrhodopsin-2. *Photochemistry and Photobiology*. 2009; 85:400–411. 1. [PubMed: 19161406]
33. Buzsáki G, Stark E, Berényi A, Khodagholy D, Kipke DR, Yoon E, Wise KD. Tools for probing local circuits: High-density silicon probes combined with optogenetics. *Neuron*. 2015; 86(1):92–105. [PubMed: 25856489]
34. Chen R, Canales A, Anikeeva P. Neural recording and modulation technologies. *Nature Reviews Materials*. 2017; 2:16093.
35. Berens P. CircStat: A MATLAB toolbox for circular statistics. *Journal of Statistical Software*. 2009; 31(10):1–21.
36. Mikulovic S, Pupe S, Peixoto HM, Do Nascimento GC, Kullander K, Tort ABL, Leão RN. On the photovoltaic effect in local field potential recordings. *Neurophotonics*. 2016; 3:015002. 1. [PubMed: 26835485]
37. Cardin JA, Carlén M, Meletis K, Knoblich U, Zhang F, Deisseroth K, Tsai L-H, Moore CI. Driving fast-spiking cells induces gamma rhythm and controls sensory responses. *Nature*. 2009; 459(7247):663–667. [PubMed: 19396156]
38. Im C, Seo JM. A review of electrodes for the electrical brain signal recording. *Biomedical Engineering Letters*. 2016; 6(3):104–112.
39. Bauhofer W, Kovacs JZ. A review and analysis of electrical percolation in carbon nanotube polymer composites. *Composites Science and Technology*. 2009; 69(10):1486–1498.

40. Mattis J, Tye KM, Ferenczi Ea, Ramakrishnan C, O'Shea DJ, Prakash R, Gunaydin La, Hyun M, Fenno LE, Gradinaru V, Yizhar O, Deisseroth K. Principles for applying optogenetic tools derived from direct comparative analysis of microbial opsins. *Nature Methods*. 2011; 9:159–172. 12. [PubMed: 22179551]
41. Ishizuka T, Kakuda M, Araki R, Yawo H. Kinetic evaluation of photosensitivity in genetically engineered neurons expressing green algae light-gated channels. *Neuroscience Research*. 2006; 54(2):85–94. [PubMed: 16298005]
42. Grossman N, Nikolic K, Grubb MS, Burrone J, Toumazou C, Degenaar P. High-frequency limit of neural stimulation with ChR2; Proceedings of the Annual International Conference of the IEEE Engineering in Medicine and Biology Society, EMBS; 2011. 4167–4170.

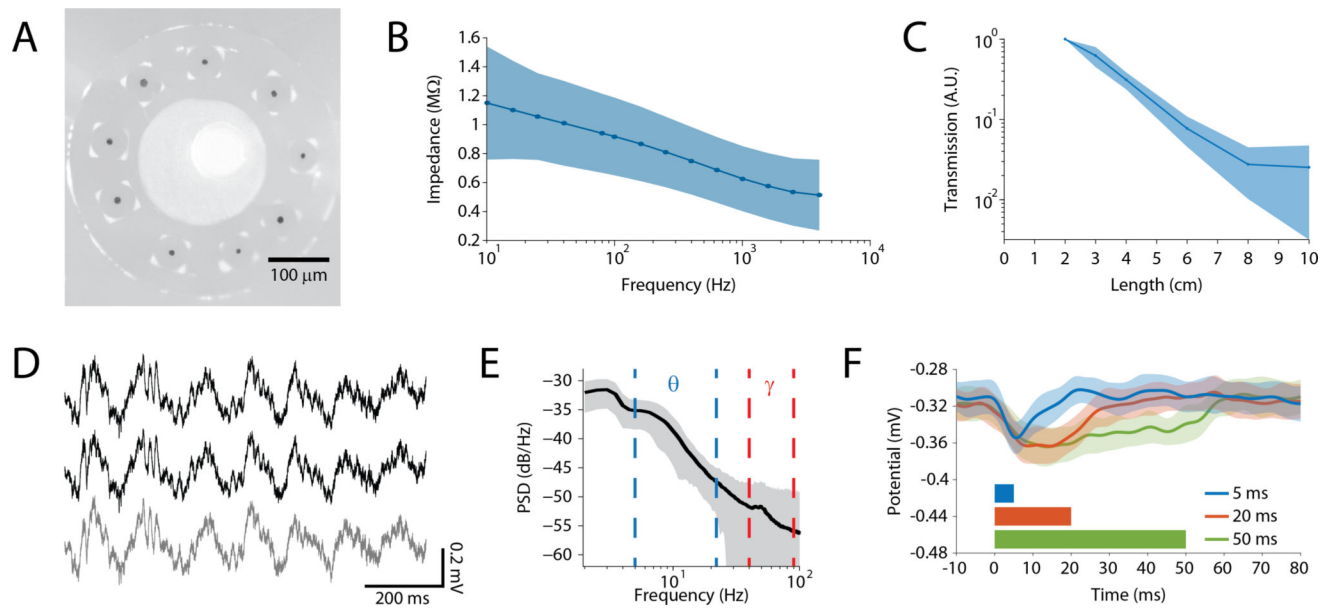


Figure 1. Hybrid fiber probes permit recording of spikes and LFPs

(A) Cross-sectional image of the hybrid probe. A ring of 9 tin recording electrodes embedded in a PEI cladding surrounding a PC-COC waveguide used for optical stimulation. (B) Impedance of the electrodes for frequencies between 10 Hz and 4 kHz, the shaded area represents standard deviation (number of electrodes $n = 6$). (C) Light transmission for different lengths of the polymer waveguide (shaded area represents standard deviation). From these results, decibel loss is determined to be 2.44 dB cm^{-1} (number of waveguides $n = 5$). (D) Spontaneous LFPs measured in a freely behaving mouse using a chronically implanted fiber. Different traces correspond to individual electrodes. (E) Power spectrum of the recordings in (D) shows that the signals were dominated by typical hippocampal theta and gamma oscillations. (F) LFP response to optical stimulation for different pulse lengths (5 ms, 20 ms, 50 ms).

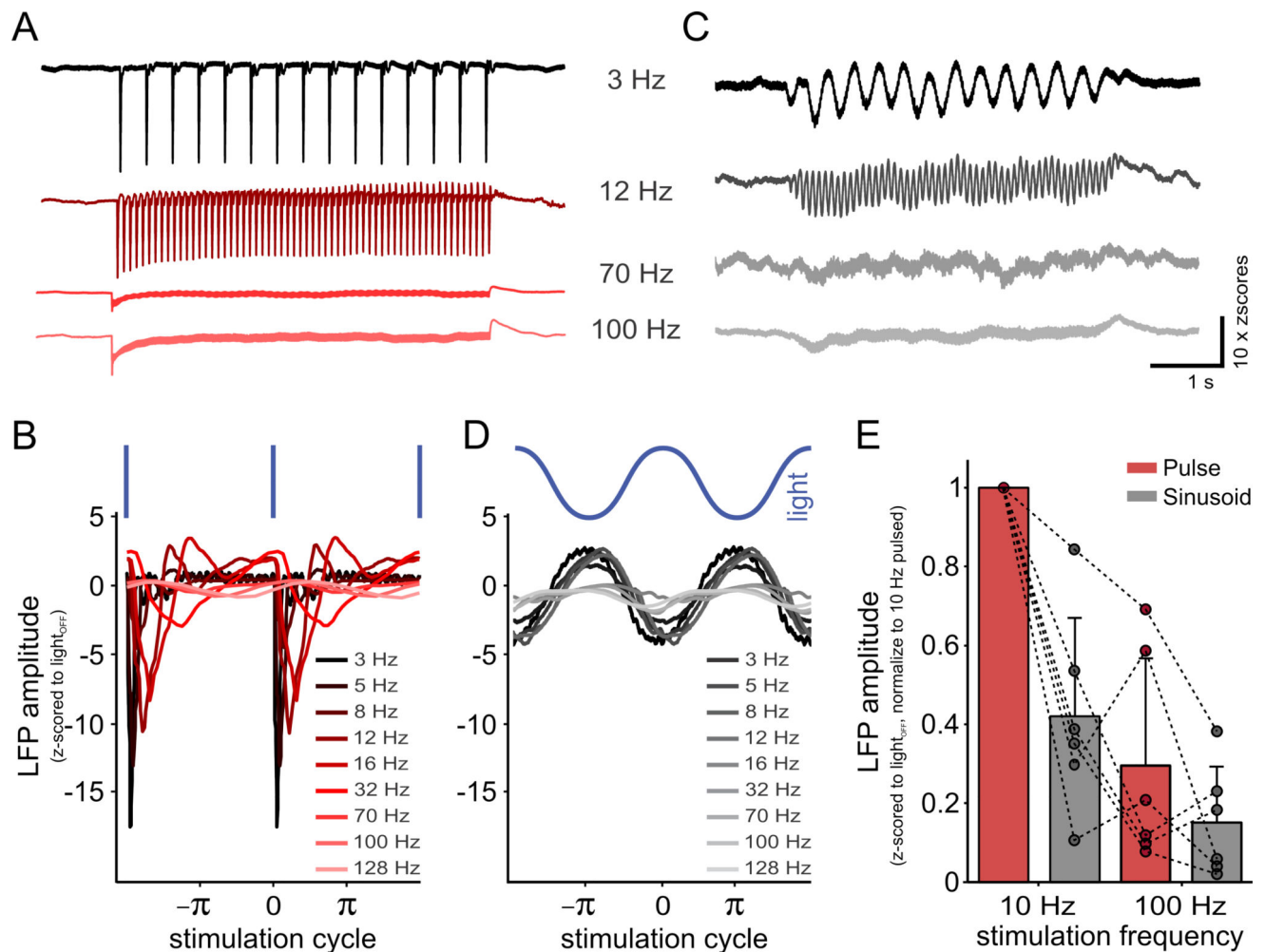


Figure 2. Sinusoidal optical stimulation enables entrainment of LFP oscillations at different frequencies

(A) Normalized averaged LFP responses to blocks of pulsed (5 ms) optical stimulation at 3, 12, 70, and 100 Hz (averaged across blocks). (B) Normalized averaged LFP response per stimulation cycle to 5 ms light pulses at frequencies of 3 – 128 Hz. (C) Analogous to (A) but following sinusoidal stimulation. (D) Normalized averaged LFP response per stimulation cycle to sinusoidal light stimulation at frequencies of 3 – 128 Hz (only cycles of full stimulus amplitudes included). (E) LFP amplitudes (peaks per stimulation cycle in C, D) were larger in response to 10 Hz than to 100 Hz optical stimulation. Pulsed (red) stimulation evoked a stronger response than the sinusoidal (gray) stimulation. LFP responses were normalized to 10 Hz pulsed stimulation in each experiment (dashed lines represent individual measurements).

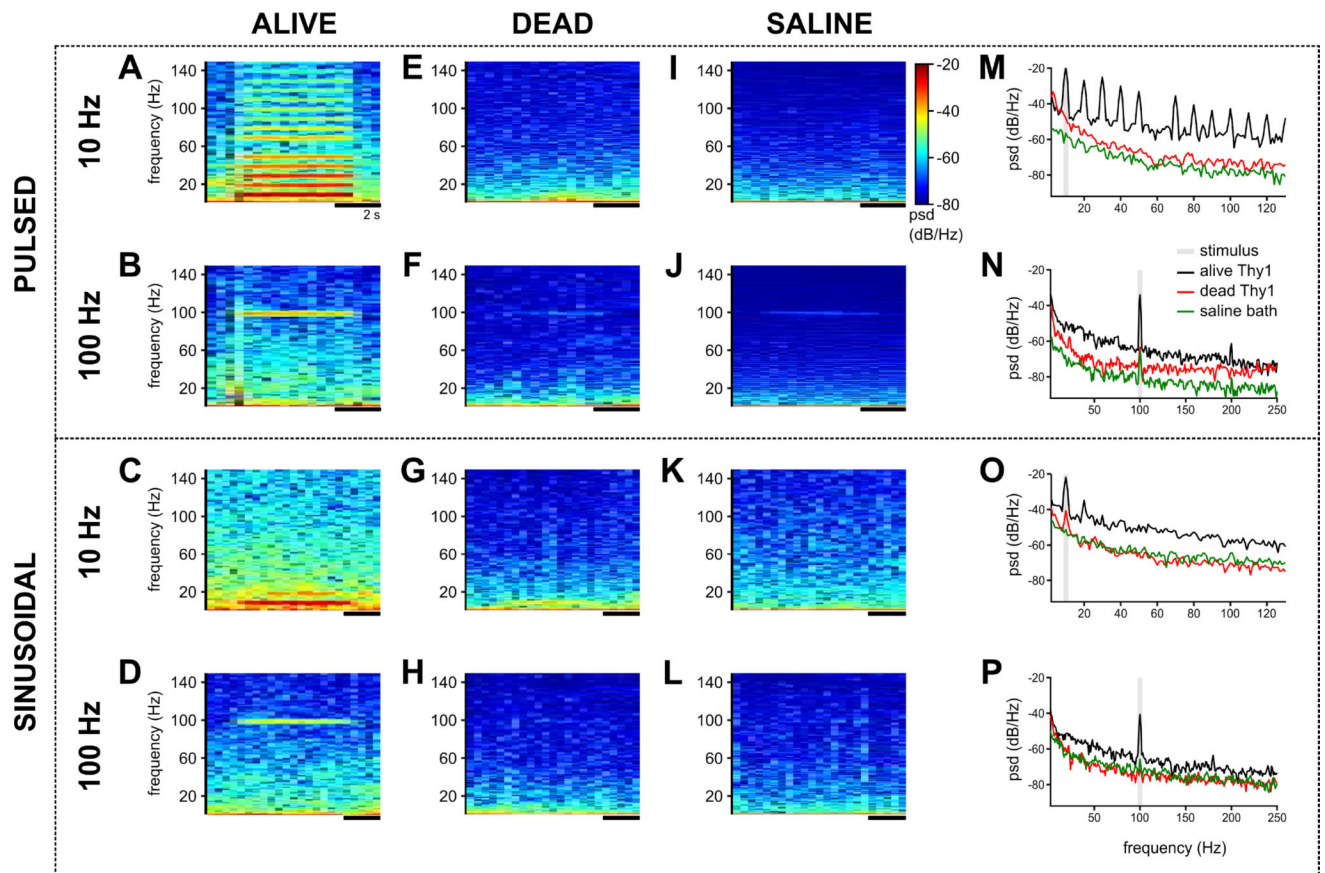


Figure 3. Neuronal signals are prevailing source of LFP responses

Spectrograms and spectra of the averaged block responses (median across 17 stimulation blocks) to 10 Hz and 100 Hz pulsed (5 ms pulses, top rows) and sinusoidal (bottom rows) light stimulation, while the probe was inserted into a Thy1-ChR2-YFP mouse (A–D) and after this mouse had been euthanized but the fiber remained in place (E–H) and while it was dipped in saline bath (I–L). All stimulation frequencies and patterns evoked a strong response in the living Thy1-ChR2-YFP mouse visible as a local maxima in the spectrogram and spectrum (M–P, black traces). After euthanizing the mouse (30 – 60 min after respiration stopped) there were no or only small potential changes in response to the stimulation left. Analogous, the spectral peaks became negligibly small (M–P, red traces). In saline bath, only 100 Hz stimulation resulted in a small spectral peak (M–P, green traces). Signals were 58–62 Hz bandstop filtered before spectral analyses. Horizontal scale bars refer to 2 s.

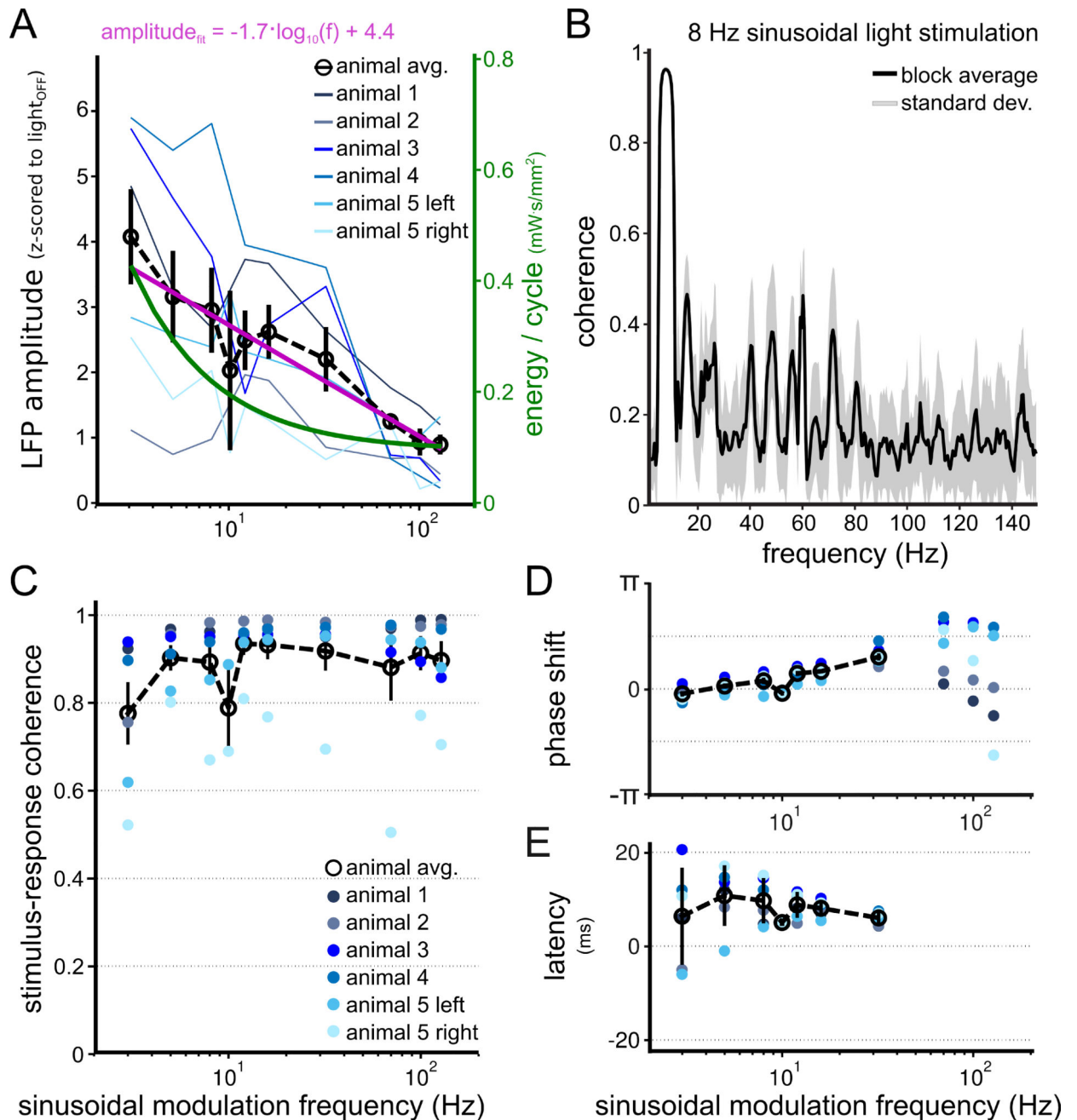


Figure 4. LFP oscillations are coherent with the oscillating light input

(A) LFP response to sinusoidal light stimulation decays exponentially with increasing modulation frequencies ($n_{\text{implantations}} = 6$; blue: normalized (z-scored to light_{OFF} periods) averaged LFP response maximum per frequency and implantation; black: mean \pm standard error of the mean over implantations; magenta: logarithmic fit to frequency response (averaged across implantations per frequency), green: averaged estimate of delivered energy per stimulation cycle and hybrid fiber ($n_{\text{fibers}} = 4$)). (B) LFP response is coherent with the light input (8 Hz sinusoidal stimulation in animal 1, coherence across 9 stimulation blocks). (C) Coherence between light input and LFP readout is on average >0.77 for all stimulation

frequencies (coherence at stimulation frequency, $n_{\text{implantations}} = 6$). **(D)** Corresponding cross-frequency phase delays increase with frequency up to 32 Hz. Greater variability is observed for 70 Hz and higher frequencies. **(E)** Temporal delays for stimulation frequencies up to 32 Hz were calculated as the time between $\text{light}_{\text{OFF}}$ and the maximum of the LFP oscillation (see Supplementary Fig. S5). Note that the maximum in the LFP corresponds to the smallest stimulation response. LFP oscillations followed the light with a delay of $\tilde{8}$ ms for all frequencies.

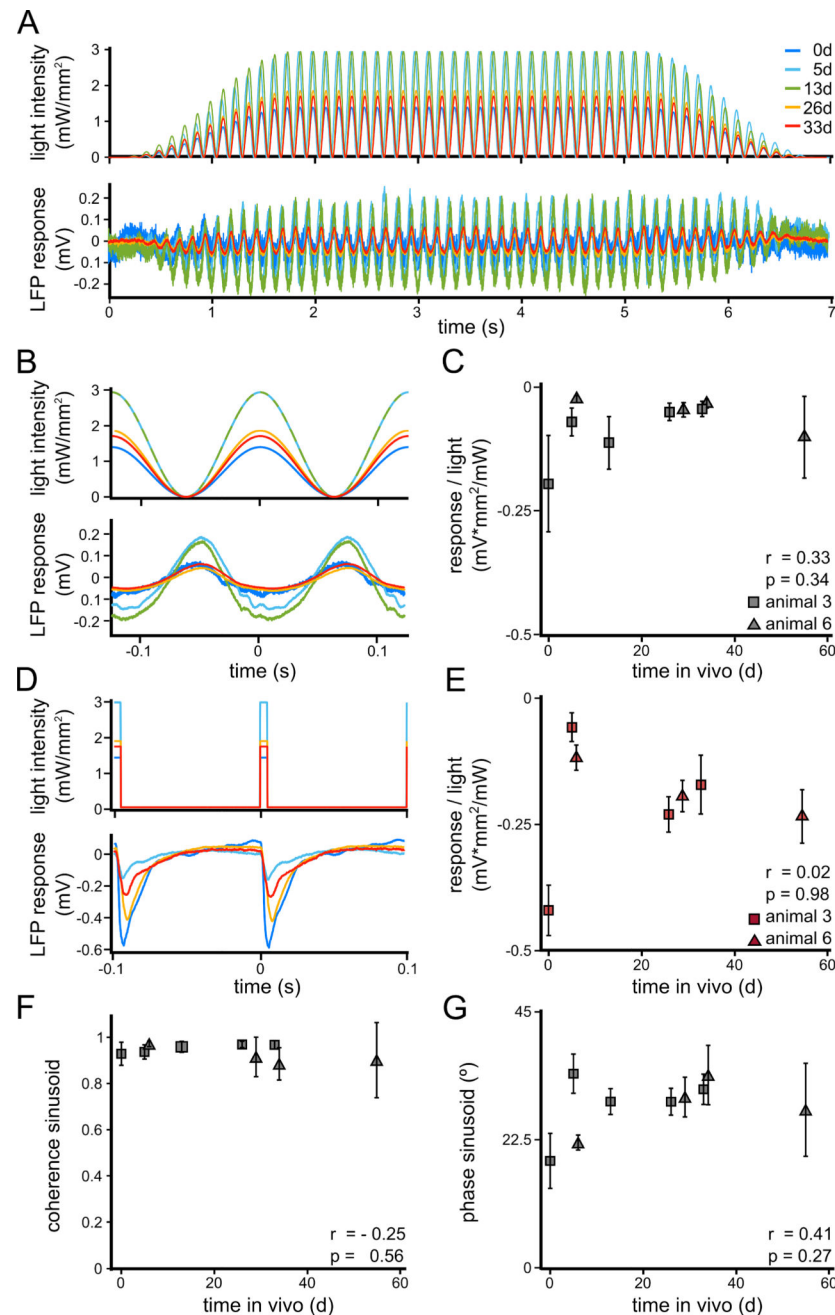


Figure 5. Hybrid fiber probes allow for chronics application of sinusoidal stimulation paradigm Sinusoidally modulated light stimulation evoked oscillating LFP responses over more than a month of implantation. **(A)** Median light input and LFP response averaged across blocks of 8 Hz stimulation. **(B)** Median light input and LFP readout averaged across stimulation cycles (n_{cycles} = 570, ramp up periods excluded). **(C)** Response amplitudes to modulated light stimulation were independent of the duration of the implantation of the hybrid fiber n_{animal} = 2, 55 days). **(D)** Pulsed optical stimulation reliably elicited LFP responses. **(E)** Median LFP response to pulsed stimulation normalized to light intensity over a period of 55 days did not show any dependence on the time period following implantation (n_{cyclesperday} = 270, 55

days). **(F)** Coherence at the stimulation frequency and **(G)** cross-spectral phase delays between LFP response and sinusoidal light input were stable over 55 days following implantation surgery.

Author Manuscript

Author Manuscript

Author Manuscript

Author Manuscript